The trimeric coiled-coil HSBP1 protein promotes WASH complex assembly at centrosomes

Sai P Visweshwaran[1], Peter A Thomason[2], Raphael Guerois[3] (iD), Sophie Vacher[4], Evgeny V Denisov[5,6] (iD), Lubov A Tashireva[7], Maria E Lomakina[8], Christine Lazennec-Schurdevin[1], Goran Lakisic[1], Sergio Lilla[2], Nicolas Molinie[1], Veronique Henriot[1], Yves Mechulam[1], Antonina Y Alexandrova[8] (iD), Nadezhda V Cherdyntseva[5], Ivan Bièche[4], Emmanuelle Schmitt[1], Robert H Insall[2] & Alexis Gautreau[1,9,*] (iD)

Abstract

The Arp2/3 complex generates branched actin networks that exert pushing forces onto different cellular membranes. WASH complexes activate Arp2/3 complexes at the surface of endosomes and thereby fission transport intermediates containing endocytosed receptors, such as α5β1 integrins. How WASH complexes are assembled in the cell is unknown. Here, we identify the small coiled-coil protein HSBP1 as a factor that specifically promotes the assembly of a ternary complex composed of CCDC53, WASH, and FAM21 by dissociating the CCDC53 homotrimeric precursor. HSBP1 operates at the centrosome, which concentrates the building blocks. HSBP1 depletion in human cancer cell lines and in *Dictyostelium* amoebae phenocopies WASH depletion, suggesting a critical role of the ternary WASH complex for WASH functions. HSBP1 is required for the development of focal adhesions and of cell polarity. These defects impair the migration and invasion of tumor cells. Overexpression of HSBP1 in breast tumors is associated with increased levels of WASH complexes and with poor prognosis for patients.

Introduction

Cells use branched actin networks to control their shape, to power cell migration, and to drive membrane remodeling in intracellular traffic (Rotty *et al*, 2013). The Arp2/3 complex is the stable multi-protein complex that generates branched actin networks. It contains two actin-related proteins, Arp2 and Arp3, and five other subunits that maintain the two actin-related proteins associated. When activated by the WCA domain of so-called nucleation promoting factors (NPFs), the Arp2/3 complex creates an actin branch (Pollard, 2007): It associates with a pre-existing actin filament and nucleates a new filament from its two subunits, Arp2 and Arp3, brought into close contact, thus mimicking a filament end (Rouiller *et al*, 2008). Such a multiprotein complex can be referred to as a molecular machine to highlight the coordinated work it performs (Alberts, 1998). No function has been ascribed to Arp2 or Arp3 in isolation, outside of the Arp2/3 complex.

Nucleation promoting factors activates the Arp2/3 complex at different subcellular locations: WAVE at the lamellipodium edge, where the branched actin network provides the force for membrane protrusion (Rotty *et al*, 2013), and WASH at the surface of endosomes, where the force generated by the branched actin network contributes to the scission of transport intermediates (Derivery *et al*, 2009b; Gomez & Billadeau, 2009). These transport intermediates either follow the retrograde route toward the Golgi (Gomez & Billadeau, 2009; Harbour *et al*, 2010) or recycle internalized receptors to the plasma membrane (Temkin *et al*, 2011; Piotrowski *et al*, 2013). The α5β1 integrin is a cargo that takes the two WASH-dependent routes, since it is recycled to the plasma membrane both from endosomes and after a detour through the trans-Golgi network

1 Ecole Polytechnique, CNRS UMR7654, Université Paris-Saclay, Palaiseau, France
2 Beatson Institute for Cancer Research, Bearsden, UK
3 Institute for Integrative Biology of the Cell (I2BC), CEA, CNRS, Université Paris-Saclay, Gif-sur-Yvette, France
4 Pharmacogenomics Unit, Department of Genetics, Institut Curie, Paris, France
5 Laboratory of Molecular Oncology and Immunology, Cancer Research Institute, Tomsk National Research Medical Center, Tomsk, Russia
6 Laboratory for Translational Cellular and Molecular Biomedicine, Tomsk State University, Tomsk, Russia
7 Department of General and Molecular Pathology, Cancer Research Institute, Tomsk National Research Medical Center, Tomsk, Russia
8 Institute of Carcinogenesis, N.N. Blokhin Cancer Research Center, Moscow, Russia
9 School of Biological and Medical Physics, Moscow Institute of Physics and Technology, Dolgoprudny, Russia
   *Corresponding author. Tel: +33 169334870; E-mail: alexis.gautreau@polytechnique.edu

(Zech *et al*, 2011; Duleh & Welch, 2012; De Franceschi *et al*, 2015; Shafaq-Zadah *et al*, 2016; Nagel *et al*, 2017). WAVE and WASH are both stably associated with four other proteins, which integrate inputs to control WCA exposure as an output (Derivery & Gautreau, 2010b; Rotty *et al*, 2013). The endosomal recruitment of the WASH complex depends on the cargo-recognition complex of the retromer (Harbour *et al*, 2012; Jia *et al*, 2012; Helfer *et al*, 2013; Gautreau *et al*, 2014). Formation of branched actin networks thus involves cascades of molecular machines.

How cells assemble these molecular machines from neosynthesized subunits is not known in most cases. Indeed, molecular machines are not just simple assemblies driven by the spontaneous association of subunits. The simple stepwise addition of subunits or subcomplexes yields a WAVE complex, where the WCA domain is not properly masked (Innocenti *et al*, 2004; Derivery *et al*, 2009a). The reconstitution of a native WAVE complex from recombinant subunits was a tour-de-force, which required a decade of work (Chen *et al*, 2014). In fact, in the cell, proteasomes exert a quality control and degrade up to 30% of neosynthesized proteins (Schubert *et al*, 2000). When one subunit of WAVE, WASH or Arp2/3 complexes is depleted, remaining subunits of the same molecular machine are usually degraded by proteasomes (Kunda *et al*, 2003; Steffen *et al*, 2006; Derivery *et al*, 2009a,b; Jia *et al*, 2010). Conversely, when an exogenous, usually tagged, subunit is overexpressed, the endogenous subunit is degraded, because its partner subunits have been titrated by the more abundant exogenous protein (Derivery *et al*, 2009a,b). These observations suggest that subunits need to assemble with their partner subunits to reach their native state and become stable (Derivery & Gautreau, 2010b). In the case of the WAVE complex, one subunit, Brk1, forms a homotrimeric precursor, even though only a single Brk1 subunit is present in the native complex (Derivery *et al*, 2008; Linkner *et al*, 2011). Brk1 turns over more rapidly than the WAVE complex, suggesting that the two Brk1 molecules that should remain after dissociation of the trimeric precursor are also degraded (Derivery & Gautreau, 2010b; Wu *et al*, 2012).

Large molecular machines, like proteasomes, require many factors for their assembly (Sahara *et al*, 2014; Budenholzer *et al*, 2017). Assembly factors transiently associate with one or several subunits, but eventually dissociate before the machine is completed. If they were to remain associated, they would be subunits. It is not yet established whether assembly factors are systematically required for the formation of smaller molecular machines, like the Arp2/3 or NPF complexes. So far, an assembly factor was only identified in the case of the WAVE complex: The Nudel protein, which transiently interacts with two subcomplexes, is critical to maintain WAVE complex levels and thus to form lamellipodia (Wu *et al*, 2012). Assembly factors offer a means to control the levels of assembled complexes. For example, starvation induces the expression of proteasome assembly factors and hence favors the assembly of new proteasomes to promote the degradation of old proteins, thereby allowing biosynthesis of new proteins in amino acid-restricted conditions (Rousseau & Bertolotti, 2016).

The Arp2/3 and the WAVE complexes are overexpressed in a variety of cancers (Molinie & Gautreau, 2018). This overexpression is usually associated with a high-grade, lymph node invasion and poor prognosis for patients (Semba *et al*, 2006; Iwaya *et al*, 2007). Since most subunits of these molecular machines are only stable within the whole complex, it means that invasive tumor cells managed to assemble more of these machines, but the mechanism involved is not known. The WASH complex, which allows focal delivery of metalloproteases and integrin recycling, is critical for tumor cell invasion (Zech *et al*, 2011; Monteiro *et al*, 2013), but whether its expression is deregulated in tumors is not known. Here, we identify the first assembly factor of the WASH complex, HSBP1, and characterize how it promotes WASH assembly. We found that HSBP1 is overexpressed in breast cancer and that its overexpression is associated with increased levels of WASH complex and poor survival of patients.

Results

Identification of HSBP1 as an assembly factor of the WASH complex

To look for putative assembly factors of the WASH complex, we derived stable 293 cell lines expressing tagged subunits of the WASH complex. We noticed a small molecular weight protein in the immunoprecipitates of CCDC53, but not of WASH, nor of Strumpellin (Fig 1A). We identified this protein as HSBP1 by mass spectrometry. The gene encoding this small protein of 76 amino acids (8.5 kDa of predicted mass) was cloned and transiently co-expressed with each subunit of the WASH complex in 293T cells. Indeed, out of the five subunits of the WASH complex, CCDC53, WASH, Strumpellin, SWIP, and FAM21, only CCDC53 interacted with HSBP1 (Fig 1B). HSBP1 is thus a possible assembly factor, because it binds to a single subunit, and not to the whole WASH complex.

To examine whether HSBP1 directly binds to CCDC53, we produced and purified these two recombinant proteins in *Escherichia coli* (Fig 1C). HSBP1 was previously crystallized, and the HSBP1 core is formed by a trimeric coiled coil (Liu *et al*, 2009). HSBP1 was, however, described as a hexamer, because the asymmetric unit of the crystal contains two trimeric coiled coils associated end-to-end. In this structure, the two trimers differ by the conformation of a bulky residue in their coiled coil, phenylalanine 27 (F27; Appendix Fig S1A). The end-to-end association of two HSBP1 trimers is a crystal-induced contact, because we found that HSBP1 in solution behaves as a homotrimer, when its mass is evaluated by size exclusion chromatography coupled to multi-angle light scattering (SEC-MALS; Fig 1D). The structure of CCDC53 was not previously characterized. We found by SEC-MALS that free CCDC53 also behaves as a homotrimer (Fig 1D). The situation is reminiscent of the distantly related Brk1 subunit of the WAVE complex (Jia *et al*, 2010): Free Brk1 exists as a homotrimer, even though a single subunit of Brk1 is present in the WAVE complex (Derivery *et al*, 2008). When CCDC53 and HSBP1 were mixed, we detected a new peak by SEC-MALS, which surprisingly corresponded to a mixed heterotrimer, containing two HSBP1 for a single CCDC53 (Fig 1D). So not only HSBP1 directly binds to CCDC53, but also this interaction remodels the quaternary structure of each component.
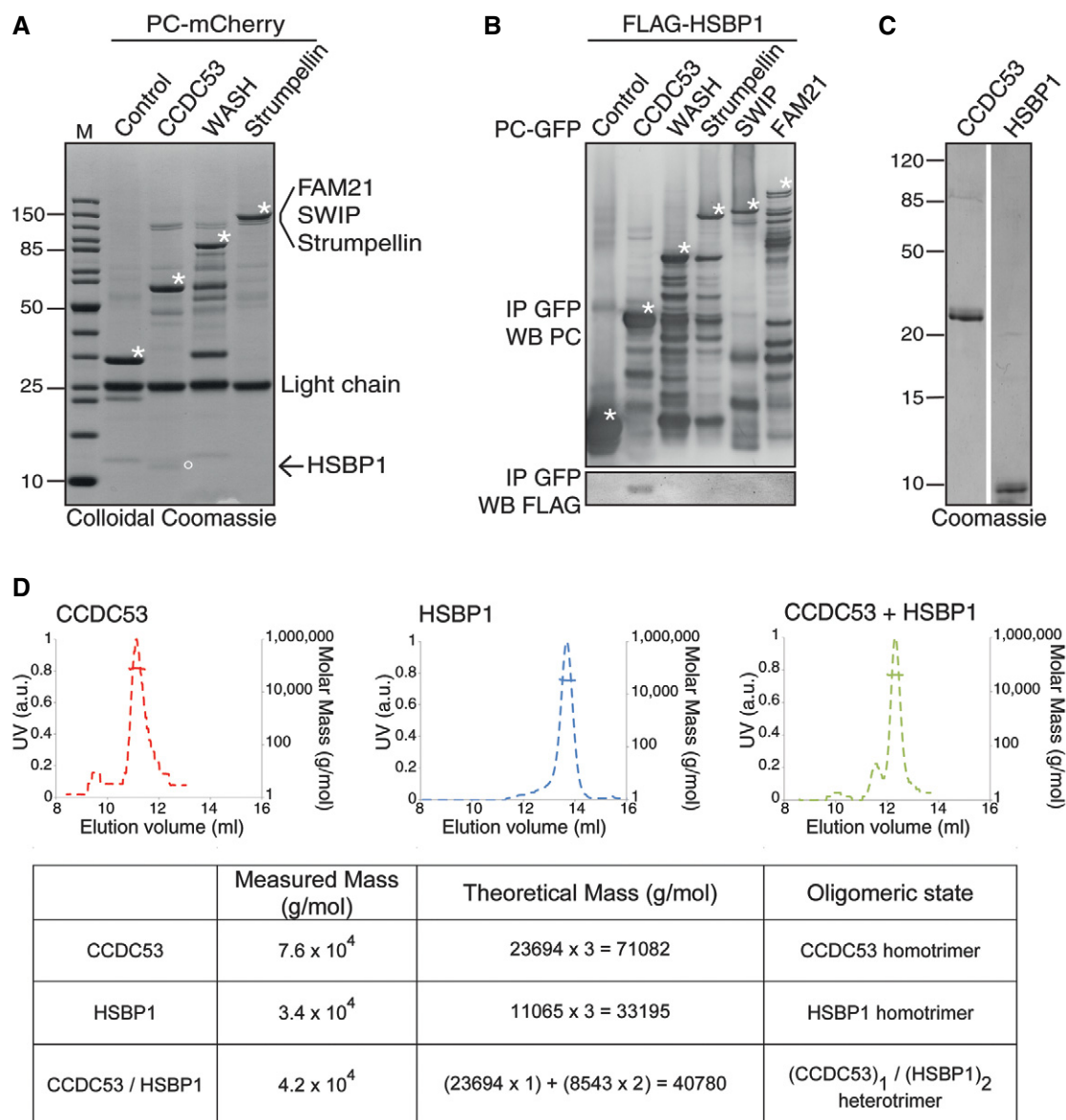
Figure 1. HSBP1 is a specific partner of the CCDC53 subunit of the WASH complex.

A   Identification of HSBP1. 293 stable cell lines expressing PC-mCherry tagged subunits of the WASH complex were subjected to PC immunoprecipitations. Immunoprecipitates were resolved by SDS–PAGE and stained with colloidal Coomassie. *indicates the precipitated bait. °indicates the position of a faint protein partner, which appears to co-immunoprecipitate with CCDC53, but not with the other WASH subunits. This protein was identified as HSBP1 by mass spectrometry. M, molecular weight markers in kDa.

B   293T cells were transiently transfected with plasmids expressing FLAG-HSBP1 and PC-GFP tagged subunits of the WASH complex as indicated. GFP precipitation of WASH complex subunits confirms the specific co-immunoprecipitation of HSBP1 with the CCDC53 subunit.

C   His-tagged full-length CCDC53 and HSBP1 were purified from *Escherichia coli*. Purity was assessed by Coomassie staining.

D   SEC-MALS analysis of CCDC53, HSBP1 or of a complex of the two proteins. CCDC53 and HSBP1 proteins are both trimeric. When mixed, His-tagged CCDC53 and untagged HSBP1 spontaneously form a heterotrimer that contains a single molecule of the CCDC53 subunit of the WASH complex.

Source data are available online for this figure.

Trimeric HSBP1 displays a distorted coiled coil. This distortion most likely arises from the accommodation of the bulky F27, which creates a steric hindrance (Appendix Fig S1A). Such a bulky residue at the d position of a coiled-coil heptad is highly unusual in trimeric coiled coils (Woolfson, 2005). However, F27 is strictly conserved in all HSBP1 homologs (Appendix Fig S1B). To better understand the reaction occurring between HSBP1 and CCDC53, we modeled the structure of free CCDC53 according to the crystal structure of free Brk1 (Linkner et al, 2011). CCDC53, whose name stands for coiled-coil domain-containing protein 53, can be modeled as a trimeric coiled-coil protein, like Brk1 (Fig 2A). Then, we used the two previous
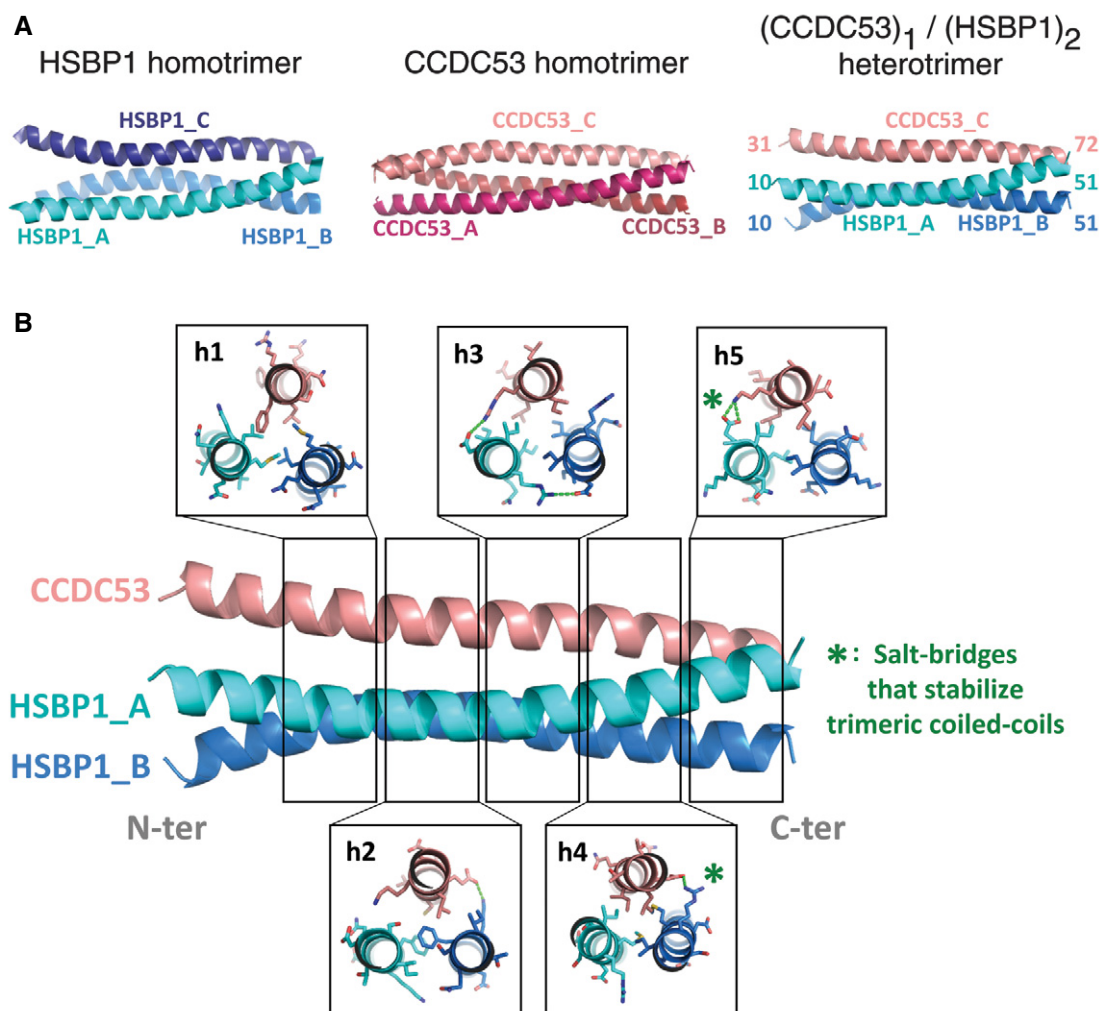
Figure 2. Structural model of the CCDC53-HSBP1 heterotrimer.

A Ribbon representation of trimeric coiled-coil assemblies formed by HSBP1, CCDC53, or the mixed heterotrimer. The HSBP1 homotrimer comes from its X-ray structure (PDB code 3CI9). The CCDC53 homotrimer is modeled based on the X-ray structure of Brk1, the distantly related subunit in the WAVE complex. The CCDC53-HSBP1 heterotrimer with 1:2 stoichiometry is modeled based on the two previous structures.

B Focus on the coiled-coil heptads of the CCDC53-HSBP1 heterotrimer. Residues buried in the trimer core of each heptad (labeled from h1 to h5) and residues that form salt bridges are shown as sticks. The E-K/R salt bridges that were shown in model systems to stabilize trimeric coiled coils are highlighted by a green asterisk in heptads 4 and 5.

structural models of HSBP1 and CCDC53 to model the mixed HSBP1-CCDC53 heterotrimer. In heptads 4 and 5 of the mixed heterotrimer, we noticed that the single strand of CCDC53 brings two optimal electrostatic couples with the two strands contributed by HSBP1 (Fig 2B). These salt bridges formed between residues E(e)-K/R(g') of heptads were identified as the most stabilizing motifs in experimental studies of model trimeric coiled coils (Roy & Case, 2009). The residues involved are strongly conserved in the sequence alignments of both HSBP1 and CCDC53 (Appendix Fig S1B). These two stabilizing salt bridges probably contribute to the spontaneous assembly of the mixed HSBP1-CCDC53 heterotrimer.

To evaluate the potential role of HSBP1 in the assembly of the WASH complex, we isolated MDA-MB-231 clones stably depleted of HSBP1 and analyzed their content in WASH complex subunits. Upon HSBP1 knock-down, steady state levels of CCDC53 and WASH, but not those of FAM21 and Strumpellin, were significantly decreased (Fig 3A). The effect of HSBP1 depletion was the same in HeLa cells upon transient transfection of siRNAs (Appendix Fig S2). The subunits of stable multiprotein complexes usually depend on each other for their stability. For the WASH complex, the depletion of a "large" subunit, such as Strumpellin, SWIP, or FAM21, induces the degradation of all remaining subunits, whereas the depletion of a "small" subunit, such as WASH or CCDC53, induces the degradation of the other small subunit, leaving intact levels of large subunits (Jia *et al*, 2010). Upon HSBP1 depletion, the co-dependent CCDC53 and WASH subunits are thus specifically downregulated.

To characterize WASH subcomplexes, we fractionated cytosolic extracts by ultracentrifugation in sucrose gradients and
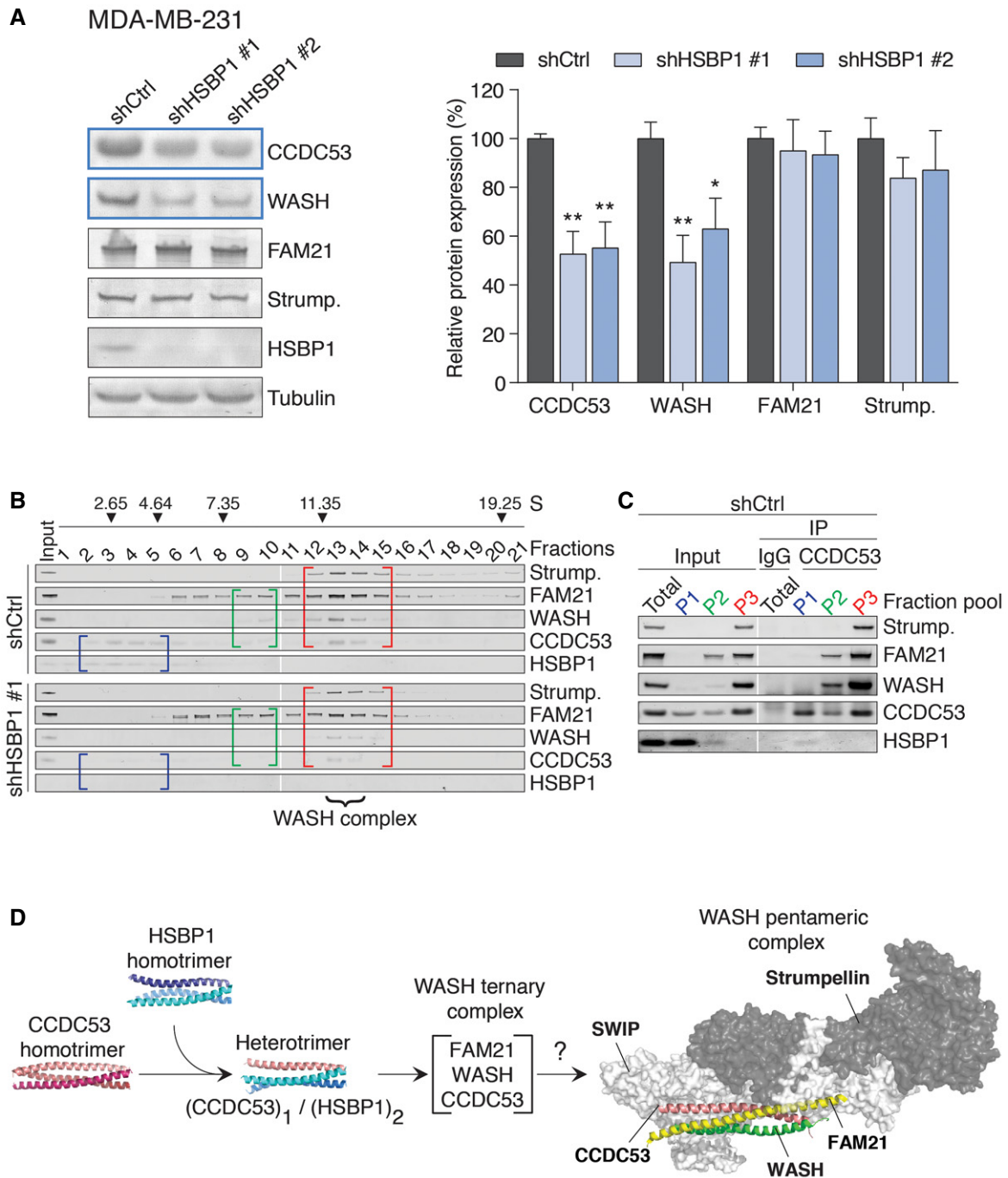
Figure 3. HSBP1 promotes the assembly of a ternary complex containing CCDC53, WASH, and FAM21.

A MDA-MB-231 clones stably transfected with plasmids expressing control or HSBP1 targeting shRNAs were obtained. HSBP1-depleted cells (shHSBP1) display significant downregulation of the CCDC53 and WASH subunits compared to control cells (shCtrl). Mean ± s.e.m. of densitometric signals; three independent experiments; ANOVA, *$P < 0.05$, **$P < 0.01$.

B Cytosolic extracts from control or HSBP1-depleted cells were fractionated by ultracentrifugation in sucrose gradients, and fractions were analyzed by Western blot with the indicated antibodies. Three color-coded pools containing CCDC53 were detected in control cells, whereas only the higher molecular weight pool was detected in HSBP1-depleted cells.

C CCDC53 immunoprecipitations of the three pools from control cells were analyzed by Western blot using the indicated antibodies. IgG refers to the control immunoprecipitation performed with non immune IgG.

D Structural model of WASH complex assembly. HSBP1 promotes WASH complex assembly by dissociating the CCDC53 homotrimeric precursor and delivering a single CCDC53 molecule to the ternary complex composed of CCDC53, WASH, and FAM21. Based on the analogous structure of the WAVE complex, a new heterotrimeric coiled coil within WASH complexes, where CCDC53, WASH, and FAM21 contribute one strand each is proposed.

Source data are available online for this figure.

analyzed the distribution of subunits in each fraction by Western blot (Fig 3B). In control MDA-MB-231 cells, we detected three distinct pools of WASH complex subunits. The low pool P1 was detected at 3.0 S, an intermediate pool P2 was detected at 8.8 S, and a high pool P3 was detected at 12.5 S, which corresponds to the previously determined sedimentation coefficient of the pentameric WASH complex (Derivery *et al*, 2009b). The P1 pool corresponds to the complex of CCDC53 with HSBP1, as determined by immunoprecipitation (Fig 3C). The P2 pool corresponds to a ternary complex containing CCDC53, WASH, and FAM21. The distribution of FAM21 in P2 is much more extended than the ones of WASH and CCDC53, suggesting that only part of FAM21 is associated with WASH and CCDC53 in the ternary complex. When HSBP1 is depleted, P1 and P2 pools of CCDC53, but surprisingly not the P3 pool, are absent. WASH is also depleted from the P2 ternary complex, but not FAM21, in line with its extended distribution. These distributions suggest that HSBP1 promotes the conversion of the CCDC53-HSBP1 heterotrimer into the CCDC53-WASH-FAM21 ternary complex.

To confirm the role of HSBP1 in promoting WASH assembly, we derived a stable MDA-MB-231 cell line that overexpresses tagged WASH. The increased WASH levels were associated with increased levels of CCDC53, but not of FAM21 and Strumpellin (Fig EV1A). When tagged WASH was overexpressed, the endogenous WASH was downregulated, as observed previously (Derivery *et al*, 2009b), suggesting that the levels of partner subunits control the total amount of WASH. In this experiment, WASH was tagged with both FLAG and HaloTag sequences. The HaloTag covalently reacts with haloalkane reactive ligands. A chemical compound called Halo-PROTAC3 induces the specific degradation of HaloTagged proteins through the recruitment of the VHL E3 ubiquitin ligase (Buckley *et al*, 2015). When cells expressing HaloTagged WASH were incubated with 1 μM HaloPROTAC3 for 24 h, levels of tagged WASH and CCDC53 significantly decreased, while endogenous WASH reappeared (Fig EV1A).

To monitor the assembly of the WASH complex, we washed out the HaloPROTAC3 compound to resume expression of HaloTagged WASH and to follow its assembly into WASH complexes by immunoprecipitation. Using this procedure, we were able to detect the buildup of WASH and associated subunits over several hours (Fig EV1B). Upon HSBP1 depletion, HaloTagged WASH associated with a reduced amount of CCDC53, but with normal amounts of FAM21 and Strumpellin, in line with the disappearance of the ternary complex (P2), but the maintenance of the pentameric complex (P3), seen in sucrose gradients.

To conceive better the sequence of events in WASH complex assembly, we then built a structural model of the pentameric WASH complex, based on the crystal structure of the analogous WAVE complex (Chen *et al*, 2010). In this model, WASH, CCDC53, and FAM21 interact through a heterotrimeric coiled coil (Fig 3D). It should be stated that the model of the WASH complex is not as robust as the one of CCDC53-HSBP1 heterotrimer, because apart from a predicted coiled-coil segment in its N-terminus, the structure of FAM21 cannot be accurately predicted. This model suggests, however, a molecular scenario where CCDC53 must be dissociated from a precursor homotrimeric form to contribute a single subunit to the ternary complex. HSBP1, which dissociates the free homotrimer of CCDC53, would deliver this single CCDC53 to WASH and FAM21.

Phenotype associated with HSBP1 depletion in MDA-MB-231 cells

Because WASH is involved in recycling α5β1 integrins from intracellular compartments to the plasma membrane, we checked the localization of this particular integrin in the stable MDA-MB-231 clones depleted or not of HSBP1. We found that α5β1 focal adhesions from HSBP1-depleted cells were strongly reduced in numbers and slightly reduced in size (Fig 4A and B). HSBP1-depleted cells display decreased levels of α5β1 integrins at their surface, as measured by FACS, and decreased total levels of β1, as measured by densitometry of Western blots (Fig 4C and D). As expected, these defects were associated with reduced adhesion to fibronectin, the major ligand of the α5β1 integrin, and to collagen type I (Appendix Fig S3). Similar defects were previously documented in WASH-depleted cells (Zech *et al*, 2011; Duleh & Welch, 2012).

MDA-MB-231 is an invasive mammary carcinoma cell line. A simple and classical assay in cancer research is the migration through pores of "transwell filters". Coating the transwell filter with a thick layer of extracellular matrix forces cancer cells to invade the gel to reach the other compartment. HSBP1-depleted cells were drastically impaired in their ability to migrate and invade through transwell filters (Fig 5A). We next examined how the HSBP1-depleted cells migrate on a 2D fibronectin substrate. When trajectories of individual cells were examined, tracks of HSBP1-depleted cells were much shorter than control ones (Fig 5B, Movie EV1). The mean square displacement highlights that HSBP1-depleted cells explore a much smaller surface area over time than controls, a direct consequence of the reduced speed and decreased directional persistence of HSBP1-depleted cells. In 3D collagen gels supplemented with fibronectin, similar defects of HSBP1-depleted cells were observed (Appendix Fig S4, Movie EV2).

To make sure that these phenotypes could be ascribed to the knock-down of HSBP1, we derived an HSBP1-depleted line re-expressing WT HSBP1. Indeed, the re-expression of HSBP1 rescued the levels of WASH and CCDC53, as well as the migration phenotype of HSBP1-depleted cells (Fig EV2, Movie EV3). We also analyzed HSBP1 mutants for their ability to rescue the phenotype. To prevent the formation of the salt bridges that stabilize the (CCDC53)$_1$/(HSBP1)$_2$ heterotrimer, we swapped charges in the R44E E49R HSBP1 mutant. To prevent the inherent distortion of the HSBP1 coiled coil, we targeted the conserved F residue in the F27L HSBP1 mutant. Both mutants were not as efficient as WT in rescuing the HSBP1 phenotype, suggesting that these HSBP1 features were important. The HSBP1 phenotype was, however, partially rescued by both mutants, a likely consequence of their overexpression.

HSBP1-depleted cells were poorly polarized, as their lamellipodium usually covers their whole periphery (Fig 6A). This defect in cell polarization was captured by their circularity index, which remains higher over several hours than one of the control cells (Fig 6B). In sharp contrast, control cells break symmetry and elongate perpendicular to the migration direction, resulting in an increased aspect ratio, the ratio of the long over the short axis. From time to time, control cells transiently lose polarity and change migration direction. The associated fluctuation in the aspect ratio is captured by the "volatility" of this parameter, an index borrowed
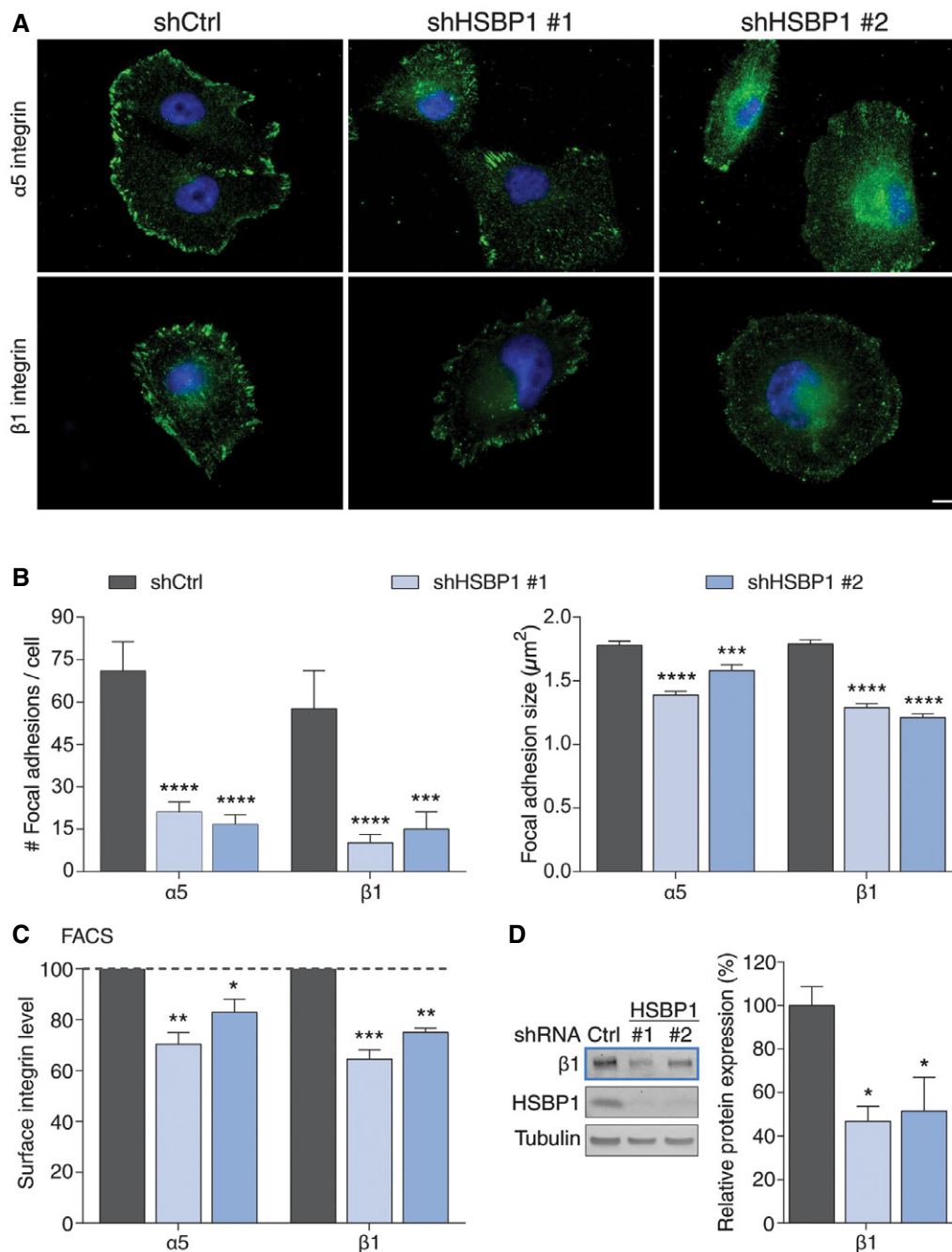
Figure 4. Integrin-mediated adhesions are decreased in HSBP1-depleted MDA-MB-231 cells.

A   HSBP1-depleted or control clones were immunostained for α5 or β1 integrins (green) and DNA (blue). HSBP1-depleted clones display a less developed array of focal adhesions. Scale bar: 10 μm.

B   HSBP1-depleted clones display a decreased number of focal adhesions per cell and of decreased size (at least 10 cells per condition, two independent experiments).

C   FACS analysis reveals reduced levels of α5β1 integrins at the surface of HSBP1-depleted clones (two independent experiments).

D   Total levels β1 integrins are decreased in HSBP1-depleted cells. Three independent measurements by densitometry.

Data information: Mean ± s.e.m.; two-way ANOVA for (B and C), ANOVA for (D), *$P < 0.05$, **$P < 0.01$, ***$P < 0.001$, ****$P < 0.0001$.
Source data are available online for this figure.

from the stock market analysis. The volatility of the aspect ratio of HSBP1-depleted cells is much lower than the one of control cells, since the lack of polarity of the latter yields a relatively constant aspect ratio close to 1 (Fig 6B). These results suggest that defective polarity of HSBP1-depleted cells or mutants can account for their impaired migration and invasion.
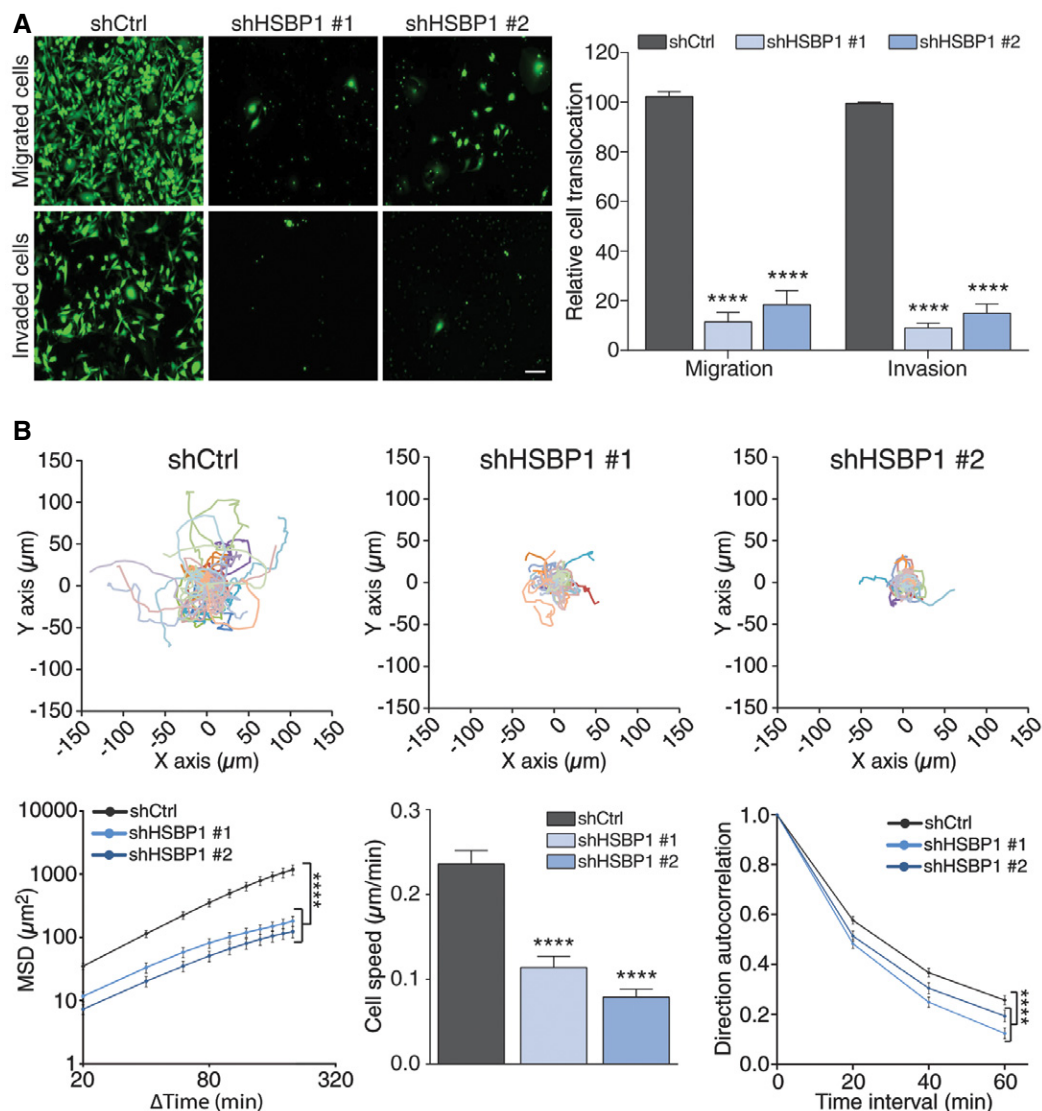
Figure 5. Impaired migration and invasion in HSBP1-depleted MDA-MB-231 cells.

A   Cell translocation through pores of transwell filters covered either with fibronectin (migration) or with a thick collagen gel supplemented with fibronectin (invasion). Four independent experiments; data are mean ± s.e.m., ANOVA, ****$P < 0.0001$. Scale bar: 50 μm.

B   Two-dimensional single cell trajectories, mean square displacement (MSD), cell speed, and directional persistence are displayed. HSBP1-depleted clones are significantly different from the control. At least 10 cells were quantified per condition, three independent experiments, data are mean ± s.e.m., ANOVA for cell speed, two-way ANOVA for MSD and directional persistence, ****$P < 0.0001$.

The role of HSBP1 is conserved in the *Dictyostelium discoideum* amoeba

HSBP1 is a well-conserved protein. We decided to knock out the orthologous gene in the amoeba *Dictyostelium discoideum*, where we had previously studied the role of the WASH complex (Carnell *et al*, 2011). To this end, we replaced the whole HSBP1 coding sequence by a selectable marker (Fig EV3A). Using a specific WASH antibody, we found that WASH is downregulated in HSBP1 KO amoebae (Fig 7A). Re-expression of HSBP1 in the KO background restored WASH levels. We then used mass spectrometry to examine the expression of the other subunits of the WASH complex. We

were able to detect and quantify specific peptides encoded by the orthologous WASH, FAM21, Strumpellin, and SWIP genes in complex extracts of amoebae (Fig 7B). The smallest subunit, CCDC53, which generates few peptides, was unfortunately not detected. HSBP1 KO induced downregulation of WASH, but not of FAM21, Strumpellin, and SWIP, as in mammalian cells. In the amoeba, WASH recruits the Arp2/3 complex at the surface of vesicles of lysosomal origin. As in WASH KO, HSBP1 KO displayed a pronounced defect in Arp2/3 recruitment at the surface of vesicles (Fig 7C).

In the presence of fluorescent dextran, which is not digestible, HSBP1 KO amoebae become "constipated" and that prevents them
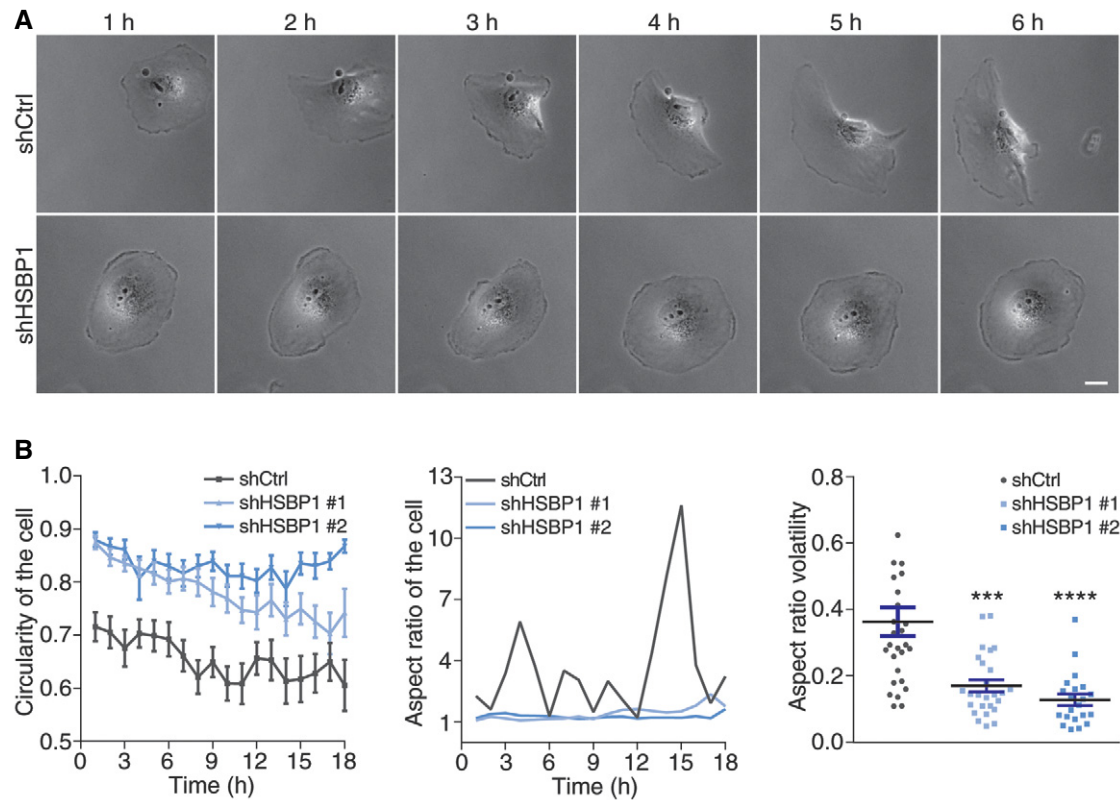
Figure 6. Decreased polarity of HSBP1-depleted MDA-MB-231 cells.

A Videomicroscopy of cells plated on a fibronectin-coated glass slide reveals that HSBP1-depleted cells are able to form a lamellipodium, but the lamellipodium they form poorly polarizes. Scale bar: 10 μm.

B At all time points, HSBP1-depleted cells remain more circular than control cells, as illustrated by the circularity index or the aspect ratio, that is, the ratio of the cell long axis over the short one. The aspect ratio of each control cell is highly irregular, as a consequence of transient loss of polarity, when the cell stops migrating. Hence the "volatility" of the aspect ratio is significantly lower in HSBP1-depleted cells, which remain unpolarized. Three independent experiments were performed with similar qualitative results. Results from the different experiments were pooled to reach at least 20 cells per conditions. Data are mean ± s.e.m.; ANOVA, ***$P < 0.001$, ****$P < 0.0001$.

from proliferating (Fig EV3B). In fact, HSBP1 KO amoebae continue to accumulate dextran well after the 2 h required for the WT amoebae to reach a steady state, when exocytosis compensates for endocytosis (Fig EV3C). When fluorescent dextran was washed out, the exocytosis defect of HSBP1 KO amoebae became obvious (Fig 7D). This phenotype of HSBP1 KO amoebae was also rescued by HSBP1 re-expression. Exocytosis involves post-lysosomal vesicles in the amoeba and requires WASH-mediated retrieval of the V-ATPase from lysosomes (Carnell *et al*, 2011). The HSBP1 phenotype is thus the same as the one displayed by WASH KO amoebae. Together, these experiments indicate that the role of HSBP1 in assembling functional WASH complexes is conserved in two distant species, human and *Dictyostelium* amoeba.

HSBP1 operates at the centrosome

To examine the localization of HSBP1 in *Dictyostelium* amoeba, we generated GFP fusion proteins at both HSBP1 ends (Fig EV3D). In both cases, HSBP1 localizes to central dot-like structures, which were identified as centrosomes using the γ-tubulin marker. We then examined HSBP1 localization by immunofluorescence of mammalian cells. In MDA-MB-231 cells, HSBP1 antibodies also brightly stained centrosomes (Fig 8A). This staining is specific because it was lost upon HSBP1 depletion (Appendix Fig S5A and B). HSBP1 staining was clearly associated with γ-tubulin, a specific marker of the pericentriolar material, but did not completely overlap with it (Appendix Fig S5C). By staining MDA-MB-231 cells expressing Halo-Tagged CCDC53 or WASH with a fluorescent HaloTag ligand, we indeed detected CCDC53 and WASH colocalized with HSBP1 and γ-tubulin at the centrosome (Fig EV4A).

To address whether HSBP1 localization to the centrosome was important for its function in promoting WASH complex assembly, we used centrinone, a Plk4 inhibitor that prevents centrosome duplication during the cell cycle (Wong *et al*, 2015). In centrosome-negative cells, HSBP1 levels were maintained, but levels of WASH complex subunits were downregulated (Fig 8B). WASH and CCDC53 signals were less intense in centrosome-negative cells, when HSBP1 was diffused, than in control cells where HSBP1 was concentrated in the centrosome (Fig 8C). These experiments suggest that HSBP1 concentration at the centrosome is important for its function in assembling WASH complexes.

To confirm the centrosomal localization of HSBP1 in tissues, we stained cryosections of normal breast and mammary
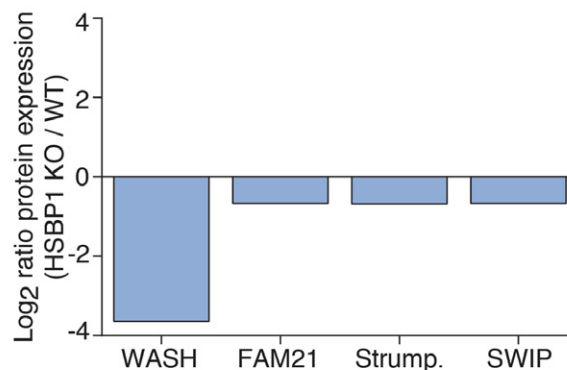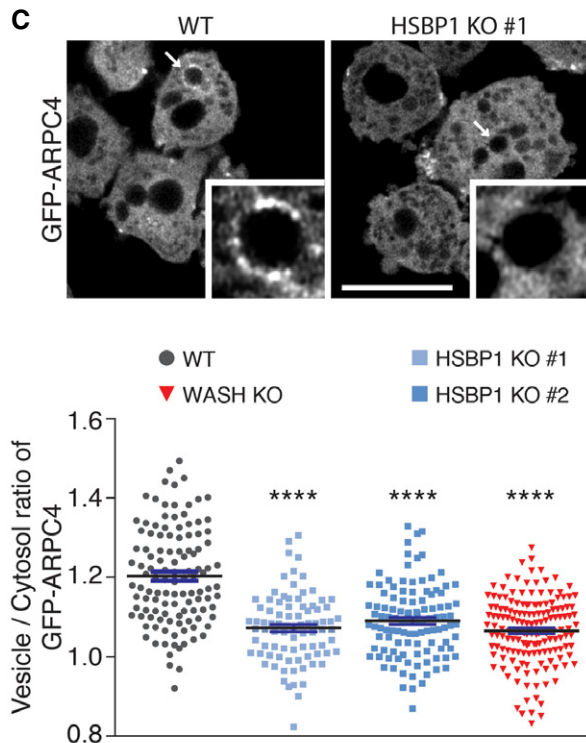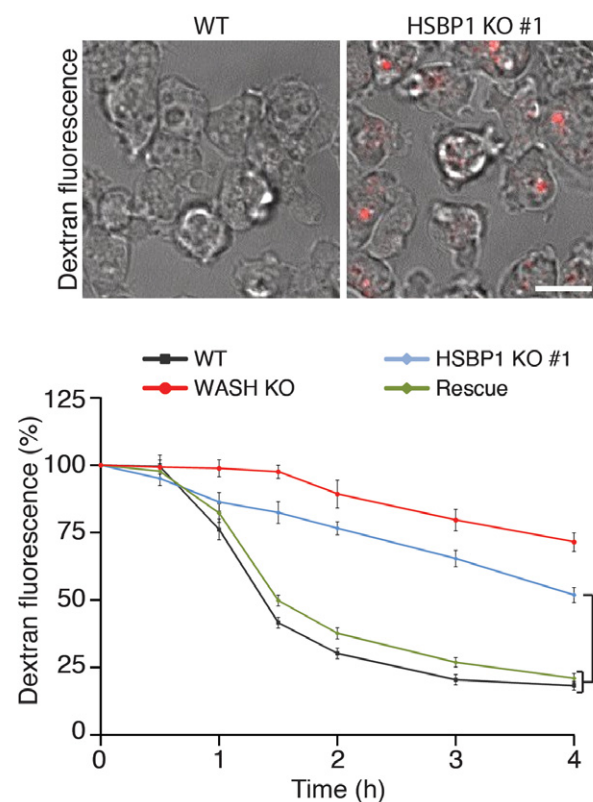
Figure 7.　The role of HSBP1 in assembling functional WASH complexes is conserved in *Dictyostelium discoideum*.

A　WASH is downregulated in the HSBP1 knock-out (KO) amoeba. This effect is rescued by HSBP1 re-expression in the KO background. The WASH KO amoeba demonstrates the specificity of the WASH antibody.

B　The indicated subunits were detected in wild-type (WT) and HSBP1 KO amoebae and their levels compared using mass spectrometry after differential labeling of tryptic peptides. WASH is specifically downregulated, when compared to the other subunits of the WASH complex, FAM21, Strumpellin, and SWIP.

C　The recruitment of the Arp2/3 complex at surface of intracellular vesicles, as observed by confocal microscopy of GFP-ARPC4, is severely impaired in HSBP1 KO amoebae, as in WASH KO amoebae. At least 80 vesicles were quantified per condition. White arrows indicate the vesicles that are zoomed. Three independent experiments, data are mean ± s.e.m., ANOVA, ****$P < 0.0001$. Scale bar: 10 μm.

D　Exocytosis of fluorescent dextran is impaired in HSBP1 KO amoebae, as in WASH KO amoebae, and is rescued by HSBP1 re-expression in the KO background. The time course of fluorescence decay indicates a profound exocytosis defect, not a mere delay. Pictures were acquired by fluorescence and DIC microscopy after 5 h of fluorescence dextran wash-out. Four independent experiments, data are mean ± s.e.m., two-way ANOVA, ****$P < 0.0001$. Scale bar: 10 μm.

Source data are available online for this figure.

carcinoma. HSBP1 staining was always partially overlapping with γ-tubulin, but appeared slightly more elongated in the presence of cilia in normal breast (Fig EV4B). Centrosomes are at the

base of cilia in normal breast, whereas these structures regress during cancer progression (Menzl *et al*, 2014). In conclusion, HSBP1 is associated with centrosomes in all case examined,
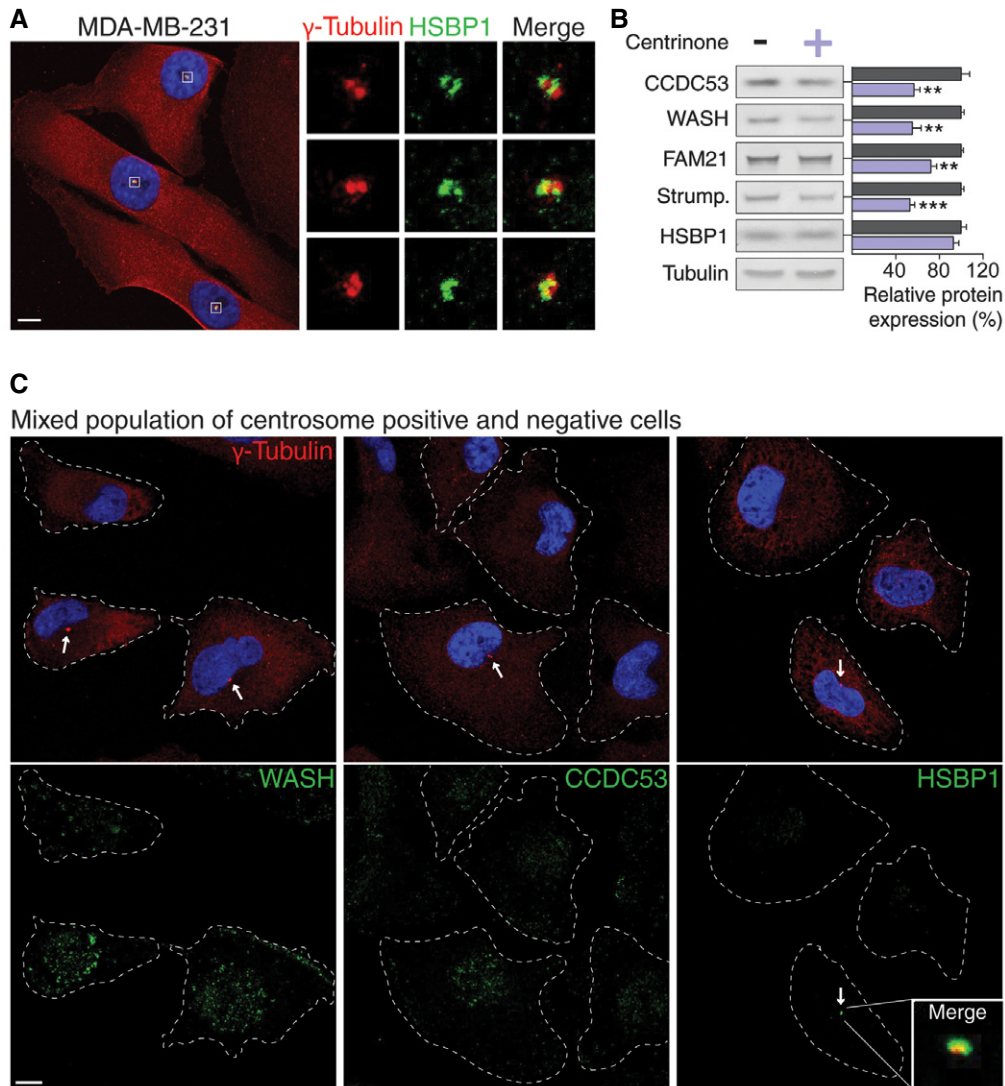
Figure 8. HSBP1 operates at the centrosome.

A MDA-MB-231 cells were stained with HSBP1 and γ-tubulin antibodies and DAPI to stain nuclei. HSBP1 is associated with the pericentriolar material stained by γ-tubulin. Scale bar: 10 μm.

B MDA-MB-231 cells were treated with centrinone, or DMSO as a control, for 20 days to generate a large population of centrosome-negative cells. Centrinone-treated cells display normal levels of HSBP1, but decreased levels of WASH complex subunits. Mean ± s.e.m. of densitometric signals; three independent experiments; paired t-test, **$P < 0.01$, ***$P < 0.001$.

C Centrinone- or DMSO-treated cells were mixed and stained for WASH, CCDC53, or HSBP1 and for γ-tubulin to identify centrosomes (white arrows). Centrosome-positive cells displayed a more intense staining for WASH and CCDC53 than centrosome-negative cells. Scale bar: 10 μm.

Source data are available online for this figure.

Dictyostelium amoeba, human cells in culture, healthy tissue, or tumors.

HSBP1 expression in breast cancer

Since the WASH complex is critical for tumor cell invasion, we examined the putative involvement of HSBP1 in the progression of breast cancer. To this end, the levels of HSBP1 mRNA were quantified in the mammary tumors of a large retrospective cohort of 446 patients, whose long-term outcome was known. HSBP1 mRNA expression significantly increased with the Scarff-Bloom-Richardson grade, which is a histological score used to evaluate cancer prognosis (Appendix Table S1). HSBP1 was also more expressed in tumors exhibiting overexpression of ERBB2. Most importantly, patients that carried tumors with a high level of HSBP1 had poor metastasis-free survival (Fig 9A).

In order to check the role of HSBP1 in WASH complex assembly *in vivo*, we examined the expression of HSBP1 and of WASH complex subunits from paired samples, which correspond to mammary carcinomas and adjacent normal tissue from the same
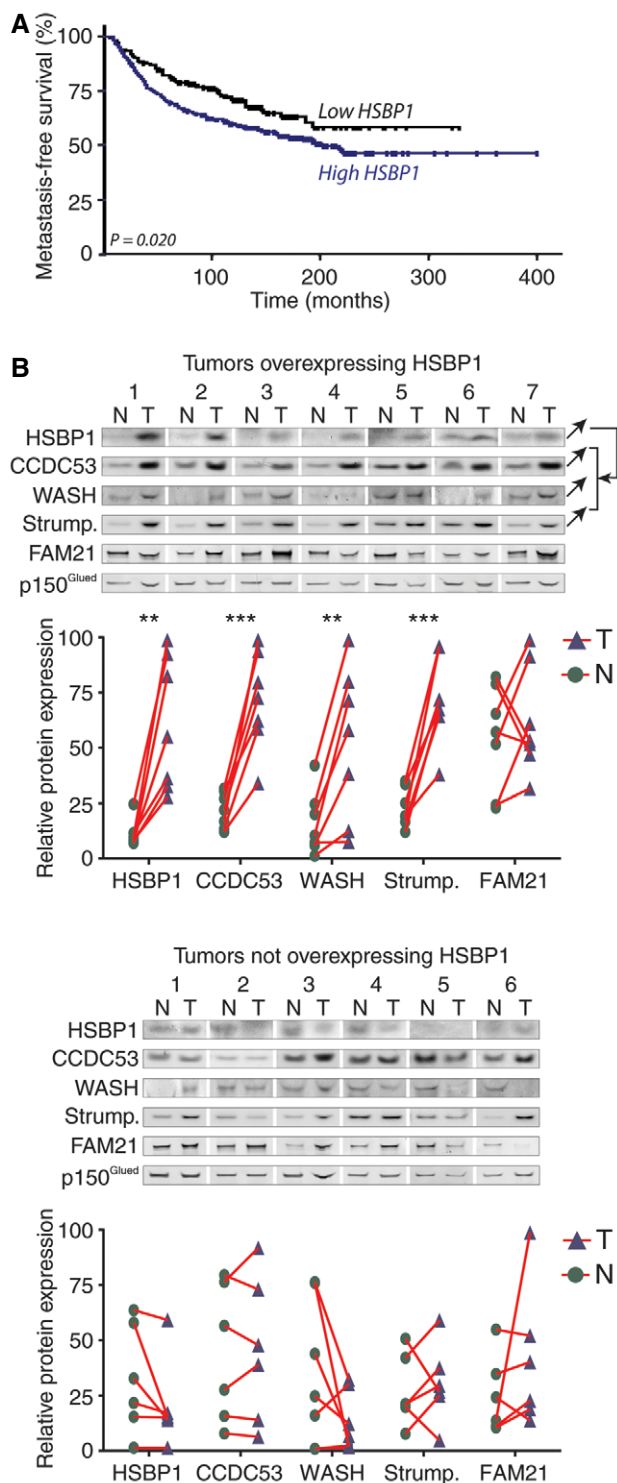
cytokeratin 7, but not stromal cells, overexpress HSBP1 and WASH complex subunits, CCDC53 and WASH (Fig EV5). In sharp contrast, the tumors that did not overexpress HSBP1 did not show overexpression of WASH complex subunits. These results obtained in patient samples suggest that HSBP1 overexpression is a means, by which in mammary carcinoma cells overexpress the WASH complex.

Discussion

We have identified HSBP1 as a specific partner of CCDC53 using proteomics and showed its involvement in WASH complex assembly. HSBP1 is the first assembly factor identified for WASH complexes. This small protein of 8.5 kDa is a negative regulator of the HSF1 transcription factor (Satyal *et al*, 1998). HSBP1 stands for HSF1 binding protein-1. HSF1 is the major transcription factor that is activated in response to heat shock. HSF1 activation involves its trimerization through a coiled coil. HSBP1 terminates HSF1 transcription in the nucleus by dissociating the active HSF1 trimer (Satyal *et al*, 1998). Here, we report a cytosolic function of HSBP1. HSBP1 can dissociate the precursor trimeric form of CCDC53 to favor WASH complex assembly. The two functions of HSBP1 thus involve a similar structural mechanism based on trimeric coiled coils. The phenotypes we report here upon HSBP1 depletion appear unrelated to the termination of the heat-shock transcriptional response.

The phenotypes we obtained here upon HSBP1 inactivation are indicative of defective WASH functions. In *Dictyostelium* amoeba, WASH knock-out produced defective Arp2/3 recruitment at the surface of lysosomal vesicles and defective exocytosis of non-digestible dextran (Carnell *et al*, 2011). In human cells, WASH depletion led to reduced surface levels of α5β1 integrins and a decreased number of focal adhesions (Zech *et al*, 2011; Duleh & Welch, 2012). WASH depletion also reduced invasive abilities of tumor cells (Zech *et al*, 2011; Monteiro *et al*, 2013). HSBP1-depleted cells also displayed a striking defect in polarity establishment that prevented them from migrating, even though they were able to generate membrane protrusions. This last phenotype was not previously reported upon WASH depletion, but it is a logical one, since the recycling of α5β1 integrins has been shown to be

patient. About half of tumors overexpressed HSBP1 at the protein level compared to normal tissue (Fig 9B). Most importantly, these tumors also exhibited increased levels of the WASH complex subunits CCDC53, WASH, and Strumpellin, but not of FAM21. We verified by immunofluorescence of formalin-fixed paraffin-embedded sections that mammary carcinoma cells, stained by

critical for migration persistence (Caswell et al, 2007; Shafaq-Zadah et al, 2016).

The analyses of WASH subcomplexes revealed several surprises. In both Dictyostelium amoeba and human cells, CCDC53 and WASH, but not Strumpellin, SWIP, and FAM21, are destabilized upon HSBP1 depletion. This is reminiscent of the fact that in RNAi-treated HeLa cells, only CCDC53 is destabilized, when WASH is depleted, and only WASH is destabilized, when CCDC53 is depleted (Jia et al, 2010). The WASH knock-out in MEF cells, however, decreased the levels of all five subunits of the WASH complex, but the remaining FAM21, SWIP, and Strumpellin subunits were still found to be associated (Gomez et al, 2012). Furthermore, we found that, by overexpressing HaloTagged WASH or by selectively destabilizing it through HaloPROTAC3 treatment, only the CCDC53 subunit mirrors the amount of WASH. Our study thus confirms the particular behavior of the interacting pair of subunits composed of WASH and CCDC53.

Surprisingly, however, our sucrose gradient analyses did not reveal a remaining FAM21–SWIP–Strumpellin subcomplex in HSBP1-depleted cells. Rather, HSBP1 appeared to specifically promote the assembly of a ternary complex of 8.8 S composed of CCDC53, WASH, and FAM21, in addition to the classical pentameric complex. Structurally, this ternary complex makes sense. We modeled that it should be organized around a heterotrimeric coiled coil, where each subunit would contribute one strand. The reason why FAM21 levels were not significantly affected upon HSBP1 depletion is probably because only a small fraction of total FAM21 is present in the ternary complex. Indeed, multiple pools of FAM21 are likely to exist, since FAM21 displays an unusually extended distribution in sucrose gradients.

The second surprise is that our subcomplex analysis supports the unexpected idea that the ternary complex, rather than the pentameric complex, carries most WASH functions. Indeed, in HSBP1-depleted cells, which exhibit a typical WASH phenotype, the pentameric complex is still present. In retrospect, the idea that the ternary complex might be the significant working molecular machine can help interpret another intriguing observation. Recently, Strumpellin knock-out cells were reported to exhibit WASH and branched actin at the surface of endosomes, like control cells (Tyrrell et al, 2016). These data put in question the role of the pentameric WASH complex. The logical assumption that the pentameric complex would derive from the ternary complex by the addition of SWIP and Strumpellin is not even clear, given that the pentameric complex is assembled around HaloTagged WASH with similar kinetics whether or not HSBP1 is present.

The localization of HSBP1 at centrosomes and the decreased levels of WASH complex in centrosome-negative cells suggests that centrosomes are sites of WASH complex assembly. Nudel, the assembly factor identified for the WAVE complex, also accumulates at centrosomes, in line with its regulatory activity toward dynein, the microtubule minus-end directed motor (Guo et al, 2006). It might be advantageous to concentrate the proteins to assemble into complexes at such a central and discrete location. One should note that many structural proteins of the centrosome are structured around large coiled coils (Kuhn et al, 2014). Even though the coiled coils we are studying here are composed of just a few heptad repeats and are of precise specificity, the concentration of coiled coils in the centrosomal area might play a role in the assembly of multiprotein

complexes. The centrosome is also a privileged site for proteasomal degradation, which is often associated with multiprotein complex assembly (Derivery & Gautreau, 2010b; Wu et al, 2012). Indeed, misfolded proteins accumulate at the centrosome through dynein-dependent transport in a structure called aggresome, when proteasomes are overwhelmed by substrates to degrade (Johnston et al, 1998; Wan et al, 2012). But centrosomes are not only sites where the WASH complex is assembled, but also sites where the WASH complex activates the Arp2/3 complex (Farina et al, 2016). The centrosomal branched actin networks are implicated in anchoring centrosomes to the nucleus (Obino et al, 2016).

HSBP1 is overexpressed in breast tumors, and its overexpression is associated with poor prognosis for patients. We documented HSBP1 overexpression in tumors compared to normal tissue in about half of patients. Fully consistent with the role of HSBP1 in assembling WASH complexes, this overexpression was associated with increased levels of WASH complex subunits. WASH overexpression in cancer was not previously reported, even if its role in tumor cell invasion was established (Zech et al, 2011; Monteiro et al, 2013). FAM21 was the only WASH complex subunit, whose levels were not correlated with the ones of HSBP1 and which was not overexpressed. FAM21 appears to have moonlighting functions, since it was found to regulate transcription by NF-κB in the nucleus independently of the WASH complex (Deng et al, 2015). In Dictyostelium amoebae, the FAM21 knock-out phenotype is also quite different from the one observed in the WASH knock-out amoeba (Park et al, 2013).

In conclusion, our study identified HSBP1 as the first assembly factor of WASH complexes, structurally characterized the step in which it functions, and established that HSBP1-mediated assembly provides a mechanism for overexpressing WASH complexes in tumors.

Materials and Methods

Information on patients, biopsies, and qRT–PCR analyses can be found in Appendix Supplementary Methods.

Plasmids

All the human open reading frames (ORFs) were flanked by FseI and AscI sites for easy shuttling between compatible plasmids. Human HSBP1 was amplified by PCR from cDNA clones IMAGE:3010737. The WASH complex subunits CCDC53, Strumpellin, and SWIP were amplified by PCR using the respective cDNA clone IMAGE:4272385, IMAGE:30532658, and IMAGE:8143997. WASH was previously cloned similarly (Derivery et al, 2009b; Helfer et al, 2013). HSBP1 mutations F27L and R44E E49R were introduced by gene synthesis (Eurofins Genomics). All PCR-amplified genes and synthesized genes were verified by sequencing. ORFs were subcloned into the following custom-made plasmids:

- a modified pET28b for the expression in E. coli. This plasmid tags the proteins with a His tag and a TEV cleavage site (MGSSHHHHHHSSGENLYFQGRP);
- pcDNAm FRT PC-GFP Blue (Derivery et al, 2009b) and pcDNAm FRT PC-mCherry Blue (Helfer et al, 2013) for expression of GFP

or mCherry tagged proteins at their N-terminus and the easy isolation of Flp-In cell lines (Derivery *et al*, 2009a);

- MXS EF1Flag HaloTag Blue SV40pA PGK PuroR bGHpA for the expression of proteins tagged at their N-terminus with FLAG and HaloTag;

- MXS EF1Flag Blue SV40pA PGK Blasti bGHpA for the expression of proteins tagged at their N-terminus with FLAG, used in rescue experiments.

The shRNA-expressing pGIPZ plasmids, non-targeting control (RHS4346), shHSBP1 #1 (V3LHS_368660, TTATCTTGCATCTGCTGCA, ORF), shHSBP1 #2 (V3LHS_409720, TGAATAGCACAACTGACCA, 3′UTR, used for rescue experiments) were obtained from Dharmacon.

Protein purification and SEC-MALS

His-tagged CCDC53 and HSBP1 were purified from *E. coli* BL21 Rosetta pLacI-Rare (Merck, Novagen), grown in 2× YT containing 25 μg/ml of kanamycin and 34 μg/ml of chloramphenicol. Cultures were induced overnight at 37°C with 1 mM IPTG, and growth was continued for 4 h at 18°C. Tagged CCDC53 and HSBP1 were retained on a Talon affinity resin (Clontech) equilibrated in buffer A (10 mM HEPES pH 7.5, 500 mM NaCl, 3 mM 2-mercaptoethanol, 0.1 mM PMSF, 0.1 mM benzamidine), eluted with buffer A containing 125 mM imidazole and further purified by gel filtration on a Superdex 200 column (10/300; GE Healthcare) equilibrated in buffer B (10 mM HEPES pH 7.5, 200 mM NaCl, 3 mM 2-mercaptoethanol, 0.1 mM PMSF, 0.1 mM benzamidine). Pure fractions were pooled and concentrated to 10 mg/ml. To purify the HSBP1-CCDC53 complex, an extract from His-tagged CCDC53-expressing *E. coli* cells was mixed with an extract from *E. coli* expressing untagged HSBP1 and purified as described above, except that the mixed heterotrimer was eluted with only 10 mM imidazole. Superdex 200 increase column (10/300; GE Healthcare) coupled to multi-angle static light scattering (SEC-MALS, Wyatt). Light scattering and refractive index measurements were performed with a MiniDAWN TREOS device (Wyatt technology) and a RID-20A (Shimadzu), respectively. Molecular mass and hydrodynamic radius calculations were performed with the ASTRA 6.1 software (Wyatt Technology) using a *dn/dc* value of 0.183 ml/g.

Antibodies, immunoprecipitations, and Western blots

Polyclonal antibodies targeting CCDC53 and FAM21 were obtained by immunizing rabbits with full-length CCDC53 and the FAM21 (1196–1341) fragment and affinity purified on a column coupled to the immunogen. Polyclonal antibodies directed against human and *Dictyostelium* WASH were previously described (Derivery *et al*, 2009b; Carnell *et al*, 2011).

Strumpellin polyclonal antibodies (C-14) were from Santa Cruz Biotechnology. HSBP pAb (Prestige HPA028940 used for IF and IHC), HSBP1 mAb (clone 2C3 used for WB), anti-FLAG mAb (Clone M2), and anti-γ-tubulin mAb (Clone GTU-88) antibodies were from Sigma-Aldrich. Integrin α5 mAb (clone VC5), integrin β1 mAb (clone 18/CD29 used for WB), p150^Glued (clone 1) were from BD Biosciences. Integrin β1 mAb (clone 12G10 used for IF and FACS) was from Abcam. Cytokeratin 7 mAb (clone N-20) was from Santa

Cruz Biotechnology. Tubulin monoclonal antibody (clone E7) was obtained from Developmental Studies Hybridoma Bank. The protein-C monoclonal antibody recognizing the PC tag (clone HPC4) was from Roche.

Immunoprecipitations were performed using resin directly coupled to HPC4 Protein-C monoclonal antibody (Roche), FLAG M2 beads (Sigma), or GFP-trap beads (Chromotek). Beads were incubated in the lysates prepared in RIPA buffer (10 mM HEPES, 50 mM NaCl, 1% NP-40, 0.5% DOC, 0.1% SDS, pH 7.7) and washed with the same buffer. HSBP1 was identified by nano LC-MS/MS as previously described (Schlüter *et al*, 2014). For WB analysis of total β1 integrin levels, cells were lysed with (50 mM Tris, 150 mM NaCl, 1.5% octylglucoside, 1% NP-40, 1 mM EDTA, pH 7.4). SDS–PAGE was performed using 4–12% Bis-Tris Nupage gels (Thermo Fischer scientific), and proteins were transferred onto nitrocellulose membranes (Protran BA85; 0.45 μm; Sigma) using liquid transfer (Criterion blotter, Bio-Rad) with sodium carbonate transfer buffer (6.25 mM NaHCO$_3$, 4.3 mM Na$_2$CO$_3$, 20% ethanol, pH 9.5). To reveal the small protein HSBP1, we optimized the Western blot protocol: It involved 30 min of in gel renaturation in (20% glycerol, 50 mM Tris–HCl, pH 7.4); after the transfer, proteins were cross-linked to the membrane using a 30-min incubation in PBS containing 0.4% paraformaldehyde. Blots were developed with alkaline phosphatase-coupled antibodies (Promega) and NBT-BCIP as substrates (Promega) or horseradish peroxidase (HRP)-coupled antibodies (Sigma) and SuperSignal West Pico chemiluminescent substrate (Thermo Fisher Scientific). Signals were then quantified by densitometry of product deposition on membranes or by photon counting (ChemiDoc imaging system, Bio-Rad).

Mammalian cells and transfections

MDA-MB-231 parental cells (ATCC HTB-26) and MDA-MB-231 shRNA clones were grown Leibovitz's L-15 medium. It was later found that MDA-MB-231 cells grew much faster in MEM medium and cells expressing HaloTag tagged CCDC53 or WASH were grown and selected in MEM medium. 293T, HeLa, and Flip-In 293T cells (Thermo Fisher Scientific) were grown in DMEM. All media were supplemented with 10% FBS. Media and serum were from Thermo Fisher Scientific. Cells were incubated in 5% CO$_2$ except cells in cultured in Leibovitz's L-15 medium, which were grown with no CO$_2$. All cells and stable clones were regularly tested for mycoplasma infection using a sensitive PCR assay and found to be negative. The vast majority of MDA-MB-231 cells were centrosome-negative after 20 days of centrinone treatment (LCR-263, 125 nM). The medium was changed every 3 days, and DMSO was used as a control.

For transient HSBP1 knock-down, HeLa or MDA-MB-231 cells were transfected with non-targeting siRNA (siZerosense; Sigma) or HSBP1 targeting siRNA (siHSBP1# 1—SASI_Hs01_00232421, GAGAAUUGAUGAUAUGAGU, siHSBP1# 2—SASI_Hs01_00232417, CAAGAUACCUGCCACGCAA, siCtrl—siZerosence, UAGCAAUGACGAAUGCGUA; Sigma) using lipofectamine RNAiMax (Thermo Fisher Scientific) and examined after 2 days. 293T cells were transiently transfected using calcium phosphate precipitation. Stable transfectants of Flip-In 293T cells were obtained by homologous recombination at the FRT site as previously described (Derivery & Gautreau, 2010a). To isolate stable clones depleted of HSBP1 or expressing

HaloTagged proteins, MDA-MB-231 cells were transfected with appropriate plasmids using Lipofectamine 2000 (Thermo Fisher Scientific) and selected with 2 μg/ml puromycin (Invivogen). For rescue experiments, MDA clones expressing the shRNA #2, targeting HSBP1 3′UTR, were transfected with plasmids expressing WT or mutant HSBP1 and selected with 2 μg/ml Puromycin and 12 μg/ml Blasticidin (Invivogen). Clones were isolated with cloning rings and expanded.

Sucrose gradient

The whole procedure is described in detail in Gautreau *et al* (2004). Briefly, cytosolic extracts were prepared by lysing cells by nitrogen cavitation (Parr instruments, 500 Psi for 20 min), followed by low speed centrifugation (16,000 × *g*, 10 min) and ultracentrifugation (150,000 × *g*, 60 min). Samples were normalized according to protein concentration determined by the BCA assay (Thermo Fisher scientific). 200 μl of extract was loaded on top of the 11 ml 5–20% sucrose gradient and ultracentrifuged for 17 h in the swinging bucket rotor SW41 Ti (Beckman) at 197,000 ×*g*. 0.5 ml fractions were collected and either concentrated by using trichloroacetic acid precipitation with insulin as a carrier for direct WB analysis or pooled for immunoprecipitation with 10 μl of Protein A/G beads (Thermo Fisher Scientific) and 1 μg of CCDC53 antibody or control IgG. NP-40 was added to a final concentration of 0.05% to avoid bead sticking. Beads were washed four times with XB buffer supplemented with 0.05% NP-40 and analyzed by WB.

Mammalian cell assays

Cell adhesion assays are performed with cells detached with 2 mM EDTA in PBS and plated in 96-well plates previously coated with 10 μg/ml of collagen-I (BD Bioscience), fibronectin (Sigma), or heat-denatured BSA (Sigma) as a negative control for background subtraction. Cells were allowed to adhere for 45 min at 37°C, non-adherent cells were washed using PBS, and adherent cells were estimated using the MTS reagent (Promega).

Two-dimensional cell migration was performed on glass-bottomed μ-Slide (Ibidi) coated with 10 μg/ml fibronectin. In three-dimensional cell migration, cells were sandwiched between two collagen gels (2 mg/ml collagen-I, 10 μg/ml fibronectin, 25 mM Hepes, 10% FBS, in DMEM) polymerized in glass-bottomed μ-Slide at 37°C for 1 h.

Transwell assays were performed using Transwell inserts (FluoroBlok, Corning) either coated with 10 μg/cm² fibronectin (migration) or with a collagen gel containing fibronectin as described above. Cells were incubated in serum-free medium and attracted to the other side of the filters by 10% serum. Cells were stained with calcein AM (Thermo fischer Scientific), and cells were imaged without fixation.

Immunofluorescence and FACS

Cells were fixed with 2% paraformaldehyde and permeabilized with 0.25% Triton X-100 for integrin staining. Cells were fixed with cold (−20°C) methanol-acetone (1:1) for HSBP1 (pAb) and γ-tubulin staining. To label HaloTagged CCDC53 or WASH, cells were incubated for 15 min in growth media containing the TMR ligand (5 μM, Promega). Cells were then rinsed twice with PBS and incubated in fresh media for 30 min to decrease background staining. Cells are then washed with PBS, then fixed with 2% paraformaldehyde, and permeabilized with cold (−20°C) methanol-acetone (1:1).

For immunofluorescence on tissue section displayed in Fig EV4, biopsies were frozen in liquid nitrogen and serially sectioned. Sections were fixed with methanol-acetone. For immunofluorescence on tissue section displayed in Fig EV5, 7-μm-thick sections were prepared from FFPE tumor samples, deparaffinized, rehydrated, processed for heat-induced epitope retrieval in PT Link (Dako) with EDTA buffer (pH 8.0), and blocked with 3% BSA in PBS. For FACS analysis, cells were fixed with 2% paraformaldehyde and analyzed on a Guava easyCyte system (Millipore).

Microscopy and image analysis

Widefield imaging was performed on an Axio Observer microscope (Zeiss) equipped with a Plan-Apochromat 100×/1.40 or 63×/1.40 oil immersion objective, an EC Plan-Neofluar 40×/1.30 oil immersion objective and a Plan-Apochromat 20×/0.80 air objective, a Hamamatsu camera C10600 Orca-R² and a Pecon Zeiss incubator XL multi S1 RED LS (Heating Unit XL S, Temp module, CO₂ module, Heating Insert PS and CO₂ cover). Live cell analysis was performed as described (Dang *et al*, 2013). Confocal images were acquired on a commercial confocal laser scanning microscope (TCS SP8, Leica) equipped with an inverted frame (Leica), a high NA oil immersion objective (HC PL APO 63×/1.40, Leica), and a white light laser (WLL, Leica). Image analysis was performed with ImageJ and FIJI. Analyses of focal adhesions, cell shape, including volatility of the aspect ratio, and cell trajectories were previously described (Gorelik & Gautreau, 2014; Horzum *et al*, 2014; Lomakin *et al*, 2015; Zhang *et al*, 2016).

Computational modeling

Modeling of the CCDC53 homotrimer and of the HSBP1-CCDC53 heterotrimer was performed using the RosettaCM protocol to build and relax the trimeric structures (Song *et al*, 2013). The CCDC53 sequence was aligned on the sequence and structure of the homotrimeric Brk1 paralog (PDB code 3PP5; Linkner *et al*, 2011) following the alignment generated by the HHpred profile–profile comparison method (Söding, 2005; Alva *et al*, 2016). The probability of a correct match between CCDC53 and HSBP1 Hidden Markov Model (HMM) profiles was 99.9%. In the heterotrimer, the register of the single CCDC53 strand with respect to the two HSBP1 strands was provided by the HMM profile of CCDC53, which matches the one of HSBP1 with a probability of 93%.

The WASH complex has been modeled based on the structure of the WAVE complex (Chen *et al*, 2010). Sequence alignments for every subunit were obtained using Hhpred (Söding, 2005), and structural models, restricted to the reliable parts of the alignments, were generated with RosettaCM (Song *et al*, 2013). Only for the FAM21 subunit, a significant alignment could not be obtained with any of the WAVE complex subunits. The domain of FAM21 spanning residues 58–128 having the highest probability to fold as a coiled coil was used to model FAM21 as a heterotrimeric coiled coil in the WASH complex context.

Dictyostelium discoideum

The HSBP1 gene was disrupted in Ax2 strain by homologous recombination (Fig EV3A). Blasticidin-resistant colonies were picked and tested to lack the entire HSBP1 coding region by PCR (Fig EV3A). The HSBP1 coding region was amplified from cDNA by PCR and cloned into *Dictyostelium* expression vectors to generate pPT606 (GFP-HSBP1), pPT607 (HSBP1-GFP), pPT608 (untagged HSBP1).

Amoebae were incubated in HL5 medium in the presence of 0.5 mg/ml tetramethylrhodamine isothiocyanate (TRITC) dextran (average MW 40 kDa; Sigma) overnight in sterile flasks shaking at 100 rpm. Total fluorescence levels were acquired as previously described (Carnell *et al*, 2011). Cells expressing GFP-ARPC4 were incubated in SIH medium overnight with 2% dextran to enlarge vesicles for ease of imaging in glass bottom dishes (Mattek). Images were captured on a Zeiss 880 LSM inverted confocal microscope with Airyscan detector, using a 63×/1.4 NA objective and deconvolved using the Zen software (Zeiss).

For mass spectrometry measurements of WASH complex subunits, amoebae were boiled in 1% SDS. Lysates were reduced using dithiothreitol and subsequently alkylated with iodoacetamide. Trichloroacetic acid precipitated pellets were washed with water, resuspended in 8 M urea buffer, diluted 1–10, and digested with trypsin. Digested peptides solutions were labeled on a Sep-Pak reverse phase C18 cartridge with light and medium dimethyl. Desalted peptides were then mixed and separated by a 2.1 mm RP-HPLC column. Fractions were dried down and injected into an Orbitrap Velos mass spectrometer and acquired for 90 min each.

Statistics

Statistical analysis and plotting of the results were carried out with GraphPad software (Prism v6.01). Data are expressed as mean ± s.e.m. with respect to the number of independent experiments unless mentioned otherwise. ANOVA followed by *post hoc* Dunnett's multiple-comparison tests is performed to analyze significant differences between more than two groups. To analyze the difference between two groups, a paired Student's *t*-test was performed. Differences were considered significant at confidence levels greater than 95% (two-tailed). Four levels of statistical significance are distinguished: $*P < 0.05$; $**P < 0.01$; $***P < 0.001$; $****P < 0.0001$.

Expanded View for this article is available online.

Author contributions

SPV performed most experiments and drafted the manuscript. AG supervised the work and wrote the manuscript. RG contributed structural models. PAT and RHI contributed experiments with *Dictyostelium*. SL performed the quantitative mass spectrometry experiment using amoeba extracts. GL performed the initial proteomics experiment that identified HSBP1 as a CCDC53 partner. VH performed DNA cloning, obtained, and purified FAM21 and CCDC53 antibodies. NM and SPV performed the FACS analysis. CL-S, YM, and ES produced recombinant protein and performed SEC-MALS analysis. SV and IB contributed qRT–PCR measurements of HSBP1 in the retrospective cohort of breast cancer patients. EVD and NVC provided tumor extracts. LAT performed immunofluorescence on tumor biopsies. MEL and AYA contributed HSBP1 immunofluorescence in normal breast tissue.

Conflict of interest

The authors declare that they have no conflict of interest.

References

Alberts B (1998) The cell as a collection of protein machines: preparing the next generation of molecular biologists. *Cell* 92: 291–294

Alva V, Nam S-Z, Söding J, Lupas AN (2016) The MPI bioinformatics Toolkit as an integrative platform for advanced protein sequence and structure analysis. *Nucleic Acids Res* 44: W410–W415

Buckley DL, Raina K, Darricarrere N, Hines J, Gustafson JL, Smith IE, Miah AH, Harling JD, Crews CM (2015) HaloPROTACS: use of small molecule PROTACs to induce degradation of HaloTag fusion proteins. *ACS Chem Biol* 10: 1831–1837

Budenholzer L, Cheng CL, Li Y, Hochstrasser M (2017) Proteasome structure and assembly. *J Mol Biol* 429: 3500–3524

Carnell M, Zech T, Calaminus SD, Ura S, Hagedorn M, Johnston SA, May RC, Soldati T, Machesky LM, Insall RH (2011) Actin polymerization driven by WASH causes V-ATPase retrieval and vesicle neutralization before exocytosis. *J Cell Biol* 193: 831–839

Caswell PT, Spence HJ, Parsons M, White DP, Clark K, Cheng KW, Mills GB, Humphries MJ, Messent AJ, Anderson KI, McCaffrey MW, Ozanne BW, Norman JC (2007) Rab25 associates with alpha5beta1 integrin to promote invasive migration in 3D microenvironments. *Dev Cell* 13: 496–510

Chen Z, Borek D, Padrick SB, Gomez TS, Metlagel Z, Ismail AM, Umetani J, Billadeau DD, Otwinowski Z, Rosen MK (2010) Structure and control of the actin regulatory WAVE complex. *Nature* 468: 533–538

Chen B, Padrick SB, Henry L, Rosen MK (2014) Biochemical reconstitution of the WAVE regulatory complex. *Methods Enzymol* 540: 55–72

Dang I, Gorelik R, Sousa-Blin C, Derivery E, Guérin C, Linkner J, Nemethova M, Dumortier JG, Giger FA, Chipysheva TA, Ermilova VD, Vacher S, Campanacci V, Herrada I, Planson A-G, Fetics S, Henriot V, David V, Oguievetskaia K, Lakisic G *et al* (2013) Inhibitory signalling to the Arp2/3 complex steers cell migration. *Nature* 503: 281–284

De Franceschi N, Hamidi H, Alanko J, Sahgal P, Ivaska J (2015) Integrin traffic - the update. *J Cell Sci* 128: 839–852

Deng Z-H, Gomez TS, Osborne DG, Phillips-Krawczak CA, Zhang J-S, Billadeau DD (2015) Nuclear FAM21 participates in NF-κB-dependent gene regulation in pancreatic cancer cells. *J Cell Sci* 128: 373–384

Derivery E, Fink J, Martin D, Houdusse A, Piel M, Stradal TE, Louvard D, Gautreau A (2008) Free Brick1 is a trimeric precursor in the assembly of a functional wave complex. *PLoS One* 3: e2462

Derivery E, Lombard B, Loew D, Gautreau A (2009a) The Wave complex is intrinsically inactive. *Cell Motil Cytoskeleton* 66: 777–790

Derivery E, Sousa C, Gautier JJ, Lombard B, Loew D, Gautreau A (2009b) The Arp2/3 activator WASH controls the fission of endosomes through a large multiprotein complex. *Dev Cell* 17: 712–723

Derivery E, Gautreau A (2010a) Assaying WAVE and WASH complex constitutive activities toward the Arp2/3 complex. *Methods Enzymol* 484: 677–695

Derivery E, Gautreau A (2010b) Generation of branched actin networks: assembly and regulation of the N-WASP and WAVE molecular machines. *BioEssays* 32: 119–131

Duleh SN, Welch MD (2012) Regulation of integrin trafficking, cell adhesion, and cell migration by WASH and the Arp2/3 complex. *Cytoskeleton (Hoboken)* 69: 1047–1058

Farina F, Gaillard J, Guérin C, Couté Y, Sillibourne J, Blanchoin L, Théry M (2016) The centrosome is an actin-organizing centre. *Nat Cell Biol* 18: 65–75

Gautreau A, Ho H-YH, Li J, Steen H, Gygi SP, Kirschner MW (2004) Purification and architecture of the ubiquitous Wave complex. *Proc Natl Acad Sci USA* 101: 4379–4383

Gautreau A, Oguievetskaia K, Ungermann C (2014) Function and regulation of the endosomal fusion and fission machineries. *Cold Spring Harb Perspect Biol* 6: a016832

Gomez TS, Billadeau DD (2009) A FAM21-containing WASH complex regulates retromer-dependent sorting. *Dev Cell* 17: 699–711

Gomez TS, Gorman JA, de Narvajas AA-M, Koenig AO, Billadeau DD (2012) Trafficking defects in WASH-knockout fibroblasts originate from collapsed endosomal and lysosomal networks. *Mol Biol Cell* 23: 3215–3228

Gorelik R, Gautreau A (2014) Quantitative and unbiased analysis of directional persistence in cell migration. *Nat Protoc* 9: 1931–1943

Guo J, Yang Z, Song W, Chen Q, Wang F, Zhang Q, Zhu X (2006) Nudel contributes to microtubule anchoring at the mother centriole and is involved in both dynein-dependent and -independent centrosomal protein assembly. *Mol Biol Cell* 17: 680–689

Harbour ME, Breusegem SYA, Antrobus R, Freeman C, Reid E, Seaman MNJ (2010) The cargo-selective retromer complex is a recruiting hub for protein complexes that regulate endosomal tubule dynamics. *J Cell Sci* 123: 3703–3717

Harbour ME, Breusegem SY, Seaman MNJ (2012) Recruitment of the endosomal WASH complex is mediated by the extended 'tail' of Fam21 binding to the retromer protein Vps35. *Biochem J* 442: 209–220

Helfer E, Harbour ME, Henriot V, Lakisic G, Sousa-Blin C, Volceanov L, Seaman MNJ, Gautreau A (2013) Endosomal recruitment of the WASH complex: active sequences and mutations impairing interaction with the retromer. *Biol Cell* 105: 191–207

Horzum U, Ozdil B, Pesen-Okvur D (2014) Step-by-step quantitative analysis of focal adhesions. *MethodsX* 1: 56–59

Innocenti M, Zucconi A, Disanza A, Frittoli E, Areces LB, Steffen A, Stradal TEB, Di Fiore PP, Carlier M-F, Scita G (2004) Abi1 is essential for the formation and activation of a WAVE2 signalling complex. *Nat Cell Biol* 6: 319–327

Iwaya K, Norio K, Mukai K (2007) Coexpression of Arp2 and WAVE2 predicts poor outcome in invasive breast carcinoma. *Mod Pathol* 20: 339–343

Jia D, Gomez TS, Metlagel Z, Umetani J, Otwinowski Z, Rosen MK, Billadeau DD (2010) WASH and WAVE actin regulators of the Wiskott-Aldrich syndrome protein (WASP) family are controlled by analogous structurally related complexes. *Proc Natl Acad Sci USA* 107: 10442–10447

Jia D, Gomez TS, Billadeau DD, Rosen MK (2012) Multiple repeat elements within the FAM21 tail link the WASH actin regulatory complex to the retromer. *Mol Biol Cell* 23: 2352–2361

Johnston JA, Ward CL, Kopito RR (1998) Aggresomes: a cellular response to misfolded proteins. *J Cell Biol* 143: 1883–1898

Kuhn M, Hyman AA, Beyer A (2014) Coiled-coil proteins facilitated the functional expansion of the centrosome. *PLoS Comput Biol* 10: e1003657–13

Kunda P, Craig G, Dominguez V, Baum B (2003) Abi, Sra1, and kette control the stability and localization of SCAR/WAVE to regulate the formation of actin-based protrusions. *Curr Biol* 13: 1867–1875

Linkner J, Witte G, Stradal T, Curth U, Faix J (2011) High-resolution X-ray structure of the trimeric Scar/WAVE-complex precursor Brk1. *PLoS One* 6: e21327

Liu X, Xu L, Liu Y, Tong X, Zhu G, Zhang XC, Li X, Rao Z (2009) Crystal structure of the hexamer of human heat shock factor binding protein 1. *Proteins* 75: 1–11

Lomakin AJ, Lee K-C, Han SJ, Bui DA, Davidson M, Mogilner A, Danuser G (2015) Competition for actin between two distinct F-actin networks defines a bistable switch for cell polarization. *Nat Cell Biol* 17: 1435–1445

Menzl I, Lebeau L, Pandey R, Hassounah NB, Li FW, Nagle R, Weihs K, McDermott KM (2014) Loss of primary cilia occurs early in breast cancer development. *Cilia* 3: 7

Molinie N, Gautreau A (2018) The Arp2/3 regulatory system and its deregulation in cancer. *Physiol Rev* 98: 215–238

Monteiro P, Rossé C, Castro-Castro A, Irondelle M, Lagoutte E, Paul-Gilloteaux P, Desnos C, Formstecher E, Darchen F, Perrais D, Gautreau A, Hertzog M, Chavrier P (2013) Endosomal WASH and exocyst complexes control exocytosis of MT1-MMP at invadopodia. *J Cell Biol* 203: 1063–1079

Nagel BM, Bechtold M, Rodriguez LG, Bogdan S (2017) Drosophila WASH is required for integrin-mediated cell adhesion, cell motility and lysosomal neutralization. *J Cell Sci* 130: 344–359

Obino D, Farina F, Malbec O, Sáez PJ, Maurin M, Gaillard J, Dingli F, Loew D, Gautreau A, Yuseff M-I, Blanchoin L, Théry M, Lennon-Duménil A-M (2016) Actin nucleation at the centrosome controls lymphocyte polarity. *Nat Commun* 7: 10969

Park L, Thomason PA, Zech T, King JS, Veltman DM, Carnell M, Ura S, Machesky LM, Insall RH (2013) Cyclical action of the WASH complex: FAM21 and capping protein drive WASH recycling, not initial recruitment. *Dev Cell* 24: 169–181

Piotrowski JT, Gomez TS, Schoon RA, Mangalam AK, Billadeau DD (2013) WASH knockout T cells demonstrate defective receptor trafficking, proliferation, and effector function. *Mol Cell Biol* 33: 958–973

Pollard TD (2007) Regulation of actin filament assembly by Arp2/3 complex and formins. *Annu Rev Biophys Biomol Struct* 36: 451–477

Rotty JD, Wu C, Bear JE (2013) New insights into the regulation and cellular functions of the ARP2/3 complex. *Nat Rev Mol Cell Biol* 14: 7–12

Rouiller I, Xu X-P, Amann KJ, Egile C, Nickell S, Nicastro D, Li R, Pollard TD, Volkmann N, Hanein D (2008) The structural basis of actin filament branching by the Arp2/3 complex. *J Cell Biol* 180: 887–895

Rousseau A, Bertolotti A (2016) An evolutionarily conserved pathway controls proteasome homeostasis. *Nature* 536: 184–189

Roy L, Case MA (2009) Electrostatic determinants of stability in parallel 3-stranded coiled coils. *Chem Commun (Camb)* 2009: 192–194

Sahara K, Kogleck L, Yashiroda H, Murata S (2014) The mechanism for molecular assembly of the proteasome. *Adv Biol Regul* 54: 51–58

Satyal SH, Chen D, Fox SG, Kramer JM, Morimoto RI (1998) Negative regulation of the heat shock transcriptional response by HSBP1. *Genes Dev* 12: 1962–1974

Schlüter K, Waschbüsch D, Anft M, Hügging D, Kind S, Hänisch J, Lakisic G, Gautreau A, Barnekow A, Stradal TEB (2014) JMY is involved in anterograde vesicle trafficking from the trans-Golgi network. *Eur J Cell Biol* 93: 194–204

Schubert U, Anton LC, Gibbs J, Norbury CC, Yewdell JW, Bennink JR (2000) Rapid degradation of a large fraction of newly synthesized proteins by proteasomes. *Nature* 404: 770–774

Semba S, Iwaya K, Matsubayashi J, Serizawa H, Kataba H, Hirano T, Kato H, Matsuoka T, Mukai K (2006) Coexpression of actin-related protein 2 and Wiskott-Aldrich syndrome family verproline-homologous protein 2 in adenocarcinoma of the lung. *Clin Cancer Res* 12: 2449–2454

Shafaq-Zadah M, Gomes-Santos CS, Bardin S, Maiuri P, Maurin M, Iranzo J, Gautreau A, Lamaze C, Caswell P, Goud B, Johannes L (2016) Persistent cell migration and adhesion rely on retrograde transport of β(1) integrin. *Nat Cell Biol* 18: 54–64

Söding J (2005) Protein homology detection by HMM–HMM comparison. *Bioinformatics* 7: 951–960

Song Y, DiMaio F, Wang RY-R, Kim D, Miles C, Brunette T, Thompson J, Baker D (2013) High-resolution comparative modeling with RosettaCM. *Structure* 21: 1735–1742

Steffen A, Faix J, Resch GP, Linkner J, Wehland J, Small JV, Rottner K, Stradal TEB (2006) Filopodia formation in the absence of functional WAVE- and Arp2/3-complexes. *Mol Biol Cell* 17: 2581–2591

Temkin P, Lauffer B, Jäger S, Cimermancic P, Krogan NJ, von Zastrow M (2011) SNX27 mediates retromer tubule entry and endosome-to-plasma membrane trafficking of signalling receptors. *Nat Cell Biol* 13: 715–721

Tyrrell BJ, Woodham EF, Spence HJ, Strathdee D, Insall RH, Machesky LM (2016) Loss of strumpellin in the melanocytic lineage impairs the WASH Complex but does not affect coat colour. *Pigment Cell Melanoma Res* 29: 559–571

Wan Y, Yang Z, Guo J, Zhang Q, Zeng L, Song W, Xiao Y, Zhu X (2012) Misfolded Gβ is recruited to cytoplasmic dynein by Nudel for efficient clearance. *Cell Res* 22: 1140–1154

Wong YL, Anzola JV, Davis RL, Yoon M, Motamedi A, Kroll A, Seo CP, Hsia JE, Kim SK, Mitchell JW, Mitchell BJ, Desai A, Gahman TC, Shiau AK, Oegema K (2015) Reversible centriole depletion with an inhibitor of Polo-like kinase 4. *Science* 348: 1155–1160

Woolfson DN (2005) The design of coiled-coil structures and assemblies. *Adv Protein Chem* 70: 79–112

Wu S, Ma L, Wu Y, Zeng R, Zhu X (2012) Nudel is crucial for the WAVE complex assembly *in vivo* by selectively promoting subcomplex stability and formation through direct interactions. *Cell Res* 22: 1270–1284

Zech T, Calaminus SDJ, Caswell P, Spence HJ, Carnell M, Insall RH, Insall RH, Norman J, Machesky LM, Machesky LM (2011) The Arp2/3 activator WASH regulates α5β1-integrin-mediated invasive migration. *J Cell Sci* 124: 3753–3759

Zhang L, Luga V, Armitage SK, Musiol M, Won A, Yip CM, Plotnikov SV, Wrana JL (2016) A lateral signalling pathway coordinates shape volatility during cell migration. *Nat Commun* 7: 11714